

**Multi-Site Inhibitors for Enteric Coronavirus:  
Antiviral Cationic Carbon Dots Based on Curcumin**

Ting Du, Nan Dong, Liurong Fang, Jian Lu, Jing Bi, Shaobo Xiao, and Heyou Han

ACS Appl. Nano Mater., **Just Accepted Manuscript** • DOI: 10.1021/acsanm.8b00779 • Publication Date (Web): 12 Sep 2018Downloaded from <http://pubs.acs.org> on September 19, 2018**Just Accepted**

“Just Accepted” manuscripts have been peer-reviewed and accepted for publication. They are posted online prior to technical editing, formatting for publication and author proofing. The American Chemical Society provides “Just Accepted” as a service to the research community to expedite the dissemination of scientific material as soon as possible after acceptance. “Just Accepted” manuscripts appear in full in PDF format accompanied by an HTML abstract. “Just Accepted” manuscripts have been fully peer reviewed, but should not be considered the official version of record. They are citable by the Digital Object Identifier (DOI®). “Just Accepted” is an optional service offered to authors. Therefore, the “Just Accepted” Web site may not include all articles that will be published in the journal. After a manuscript is technically edited and formatted, it will be removed from the “Just Accepted” Web site and published as an ASAP article. Note that technical editing may introduce minor changes to the manuscript text and/or graphics which could affect content, and all legal disclaimers and ethical guidelines that apply to the journal pertain. ACS cannot be held responsible for errors or consequences arising from the use of information contained in these “Just Accepted” manuscripts.

1  
2  
3  
4 **Multi-Site Inhibitors for Enteric Coronavirus: Antiviral Cationic Carbon Dots**  
5  
6 **Based on Curcumin**  
7

8  
9 Ting Du<sup>†</sup>, Nan Dong<sup>‡</sup>, Liurong Fang<sup>‡</sup>, Jian Lu<sup>†</sup>, Jing Bi<sup>†,§</sup>, Shaobo Xiao<sup>‡,\*</sup> and Heyou  
10  
11 Han<sup>†,\*</sup>  
12

13  
14 <sup>†</sup>State Key Laboratory of Agricultural Microbiology, College of Food Science and  
15  
16 Technology, College of Science, Huazhong Agricultural University, Wuhan 430070,  
17  
18 PR China.  
19

20  
21  
22 <sup>‡</sup>State Key Laboratory of Agricultural Microbiology, College of Veterinary Medicine,  
23  
24 Huazhong Agricultural University, Wuhan 430070, PR China.  
25

26  
27  
28 <sup>§</sup>Department of Immunology and Aetology, College of Basic Medicine, Hubei  
29  
30 University of Chinese Medicine, Wuhan 430065, PR China.  
31  
32

33  
34  
35  
36  
37 ABSTRACT: The research of carbon-based antivirals is still in its infancy, and it  
38  
39 remains to be explored to develop into safe and effective carbon dots (CDs) with  
40  
41 antiviral activity at multiple points in life cycle of the virus. Here, we report a  
42  
43 one-step method to apply curcumin, to prepare of uniform and stable cationic carbon  
44  
45 dots (CCM-CDs) with antiviral properties. The inhibitory effect of CCM-CDs on viral  
46  
47 replication was studied by using porcine epidemic diarrhea virus (PEDV) as a  
48  
49 coronavirus model. Porcine epidemic diarrhea virus (PEDV) is applied as a  
50  
51 coronavirus model to study the antiviral effect of as-prepared CCM-CDs on its  
52  
53  
54  
55  
56  
57  
58  
59  
60

1  
2  
3 replication. The cationic CCM-CDs treatment is found obviously to inhibit the  
4 proliferation of PEDV compared with the common CDs (EDA-CDs). The CCM-CDs  
5 treatment can change the structure of surface protein in viruses, thereby inhibiting  
6 viral entry. And it can also suppresses the synthesis of negative-strand RNA of virus,  
7 the budding of the virus as well as the accumulation of reactive oxygen species (ROS)  
8 by PEDV. Furthermore, CCM-CDs treatment is also found to suppress viral  
9 replication by stimulating the production of interferon-stimulating genes (ISGs) and  
10 pro-inflammatory cytokines. These results offer theoretical support for the  
11 development of CCM-CDs as a hopeful antiviral drug for the treatment of coronavirus  
12 infections, including PEDV.  
13  
14  
15  
16  
17  
18  
19  
20  
21  
22  
23  
24  
25  
26

27  
28 *KEYWORDS:* curcumin, carbon dots, antiviral, interferon-stimulating genes,  
29 pro-inflammatory cytokines  
30  
31  
32  
33  
34  
35  
36  
37

## 38 **1. INTRODUCTION**

39  
40 Curcumin (CCM), a polyphenol compound obtained from turmeric roots. Due to its  
41 antioxidant, antiviral, anti-inflammatory, anticancer, antibacterial functions and so on,  
42 the potential application of curcumin in multiple industries is gaining interest.<sup>1-3</sup> Maya  
43 et al. demonstrated that curcumin inhibited the expression and multiplication of HBV  
44 by down-regulating PGC-1 $\alpha$ .<sup>4</sup> Ali et al. found that curcumin inhibited HIV-1 infection  
45 through facilitating the degradation of Tat protein and reducing Tat-mediated  
46 transcription of the TLR promoter.<sup>5</sup> Narayanan et al. evaluated the antiviral activity of  
47  
48  
49  
50  
51  
52  
53  
54  
55  
56  
57  
58  
59  
60

1  
2  
3  
4 curcumin against RVFV. And the mechanism confirmed that curcumin inhibited  
5  
6 RVFV replication by preventing phosphorylation of I $\kappa$ B- $\beta$  NSs protein in the NF- $\kappa$ B  
7  
8 pathway.<sup>6</sup> However, the pure CCM cannot be widely applied due to its insolubility in  
9  
10 physiological media and poor bioavailability *in vivo*. To overcome these shortcomings  
11  
12 of CCM, a widely used strategy is to encapsulate CCM in inorganic-based carriers,<sup>7,8</sup>  
13  
14 but the process of synthesizing these nanoparticles is relatively tedious and  
15  
16 time-consuming, furthermore, this treatment does not significantly improve the  
17  
18 antiviral activity of CCM. Thus, developing simple, safe and effective method to  
19  
20 improve the bioavailability, solubility, as well as antiviral activity is extremely  
21  
22 important.  
23  
24  
25  
26  
27  
28

29 Due to their different compositions and characteristics, nanoparticles can be  
30  
31 perfectly practiced as a carrier in efficient delivery of drugs to special sites.<sup>9,10</sup>  
32  
33 Besides, nanoparticle-based antiviral agents have been reported as potential  
34  
35 alternatives in the treatment of diseases because of their distinctive biological  
36  
37 properties derived from morphological (e.g. size, structure) and physicochemical  
38  
39 features, different from those of traditional small-molecule drugs.<sup>11,12</sup> Antiviral  
40  
41 nanomaterials, such as silver nanoparticles, functional gold nanoparticles,<sup>13,14</sup>  
42  
43 peptide<sup>15</sup> and polyvalent nanoarchitectures,<sup>16-18</sup> have aroused widespread research  
44  
45 interest.<sup>19</sup> Among the nanomaterials, silver nanoparticles (AgNPs) have the highest  
46  
47 potential for commercialization, and numerous studies have demonstrated that AgNPs  
48  
49 possess a strong antiviral activity against human immunodeficiency virus (HIV),  
50  
51 H1N1 influenza virus, herpes simplex virus (HSV) and so on.<sup>20,21</sup> The complicated  
52  
53  
54  
55  
56  
57  
58  
59  
60

1  
2  
3 antiviral mechanisms of silver nanoparticles include competing viruses binding to  
4 cells, interactions with DNA, attachment to the cell surface to change membrane  
5 characteristics, inactivating virus particles before entry and enzyme damage.<sup>22</sup>  
6  
7 However, before the adhibition of metal nanoparticles to therapeutic or preventive  
8 therapy, it is essential to assess the cytotoxicity to most human cells and the  
9 underlying long-term sequelae caused by contacted with these compounds.<sup>23,24</sup>  
10  
11 Therefore, nanoantibiotics based on non-metallic nanoparticles have appealed  
12 widespread attention owing to their outstanding antiviral characteristic. Recently,  
13 carbon-based nanomaterials have been confirmed to have potent antiviral  
14 properties.<sup>25-27</sup> Sametband et al. found that GO derivatives could suppress viral  
15 infection through competing for virus-cell binding.<sup>28</sup> Barras et al. investigated that  
16 surface functionalized carbon nanodots could function as entry inhibitors through  
17 interaction with the virus at the early stage of viral infection. Meanwhile, our previous  
18 work has demonstrated that CDs might inhibit viral replication via positively  
19 regulating antiviral type I interferon response.<sup>29</sup> In this study, a novel carbon dots  
20 from curcumin as a precursor was prepared, which could improve the bioavailability  
21 of curcumin and achieve synergistic antiviral effect.  
22  
23  
24  
25  
26  
27  
28  
29  
30  
31  
32  
33  
34  
35  
36  
37  
38  
39  
40  
41  
42  
43  
44  
45

46 In the present study, it is reported that antiviral cationic carbon dots (CCM-CDs)  
47 are prepared from herbs for the first time and it provides a novel clue to improve the  
48 antiviral activity of herbs. We find that CCM-CDs treatment can significantly inhibit  
49 viral entry, the synthesis of negative-strand RNA in virus, the budding of virus and the  
50 accumulation of reactive oxygen species (ROS) by PEDV. The antiviral activity of  
51  
52  
53  
54  
55  
56  
57  
58  
59  
60

1  
2  
3 CCM-CDs may also be ascribed to ISG proteins and pro-inflammatory cytokines  
4  
5  
6 production.  
7  
8  
9

## 10 11 12 **2. EXPERIMENTAL SECTION** 13

14  
15 **2.1. Preparation of curcumin carbon dots (CCM-CDs).** Curcumin (0.30 g)  
16  
17 and citric acid (0.60 g) were ground uniformly, sealed and hydrothermally treated in a  
18  
19 25 mL Teflonlined autoclave at 180 °C for 1 h. 15 mL ultrapure water was added to  
20  
21 the brown mixture obtained from the reaction, followed by centrifugation to eliminate  
22  
23 the large particles.<sup>30</sup> Finally, the as-prepared CDs (CCM-CDs) were dialyzed (the  
24  
25 cut-off molecular weight of the dialysis membrane was 100 D) and then kept in low  
26  
27 temperature. In the control experiment, 2.0 g citric acid was poured into 8.0 mL  
28  
29 distilled water, and then 1.0 mL ethylenediamine (EDA) was added to form a  
30  
31 homogeneous solution. Then, the mixture was reacted at 200 °C for 3 h.<sup>31</sup> The  
32  
33 obtained CDs (EDA-CDs) were also subjected to dialysis, purification, and kept in  
34  
35 low temperature.  
36  
37  
38  
39  
40  
41  
42

43 **2.2. Cytotoxicity assay.** Briefly, Vero cells were seeded and allowed to grow  
44  
45 monolayer, and then incubation with CCM-CDs (15.6-250 µg/mL) for 24 and 48 h.  
46  
47 Then CCK-8 reagent was infected and cultured for 1 h.<sup>32</sup> The relative viability of cells  
48  
49 was counted based on the expressions: cell survival rate (%) = OD(sample)  
50  
51 /OD(control) × 100%.  
52  
53  
54  
55

56 **2.3. Entry assay.** Briefly, PEDV was exposed with various concentrations of  
57  
58  
59  
60

1  
2  
3  
4 CCM-CDs (37 °C/1 h) and then added into 100% confluent Vero cells to allow the  
5  
6 entry of virions and infection for another 1 h, and then coated with medium. The cells  
7  
8 continue to be cultured until the control group shows viral lysis plaques. The viral  
9  
10 titers were measured via plaque assay.<sup>33</sup>  
11  
12  
13

14 **2.4. Penetration assay.** Vero cells were precooled (4 °C/30 min), followed by  
15  
16 infection with PEDV to allow the attachment of virions to cells at 4 °C. After  
17  
18 incubation for 2 h, medium containing different concentrations of CCM-CDs were  
19  
20 supplemented and maintaining the cells at 37 °C to start in penetration of virus for 3 h.  
21  
22 The remaining steps are consistent with the entry assay.<sup>34</sup>  
23  
24  
25  
26

27 **2.5. Viral negative-strand RNA replication.** Vero cells were infection with  
28  
29 PEDV at a MOI of 0.01 (1 h), and then co-cultured with DMEM (supplement 10  
30  
31 µg/mL trypsin) or CCM-CDs. At 5, 6, 7 and 8 hpi, the cell monolayer was harvested  
32  
33 using TRIzol reagent and the expression of PEDV negative-strand RNA was detected  
34  
35 via real-time RT-PCR according to the literature.<sup>35</sup>  
36  
37  
38  
39

40 **2.6. Release analysis.** Vero cells were inoculated with PEDV at a MOI of 0.01  
41  
42 and incubated for the specified time. Then the supernatant was discarded and cells  
43  
44 were then untreated or treatment with CCM-CDs for 15, 30, 45 and 60 min.  
45  
46 Subsequently, medium supernatants and cell lysates including progeny PEDV were  
47  
48 harvested, respectively. Viral titer of samples was tested via plaque assay.  
49  
50  
51  
52

53 **2.9. Determination of ROS production.** ROS cumulation suppressed by  
54  
55 CCM-CDs-exposed Vero cells was measured based on the previously reported.<sup>36</sup>  
56  
57  
58  
59  
60

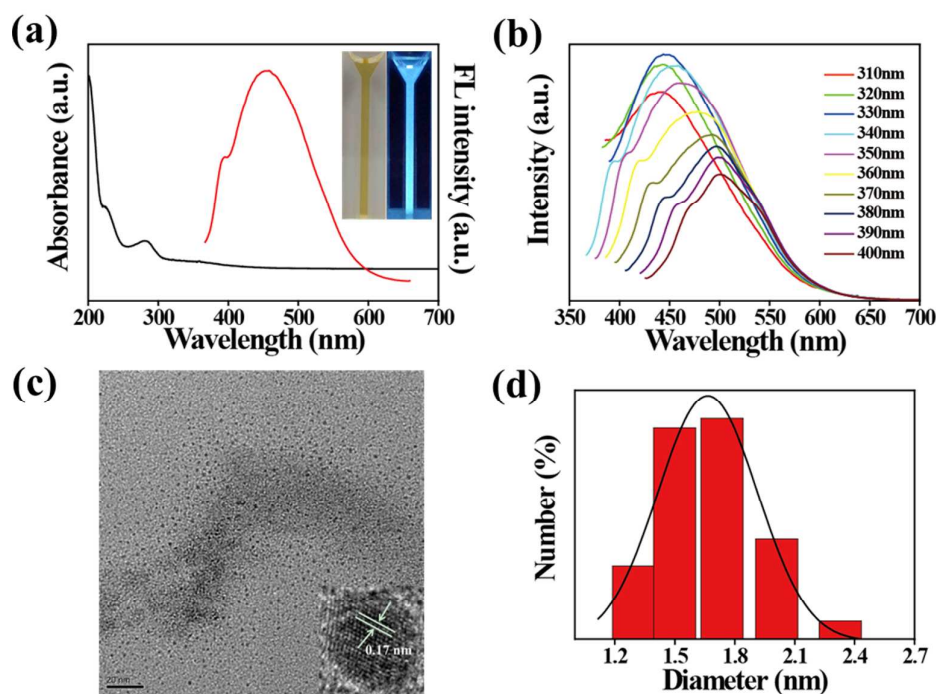
1  
2  
3 Briefly, PEDV infection of Vero cells was performed by preincubation with 10  $\mu$ M  
4 DCF (30 min/37  $^{\circ}$ C), and then treatment with CCM-CDs for 12 h. The ROS level was  
5  
6 visualized by a confocal laser scanning microscope.  
7  
8  
9

10  
11 **2.10. Statistical analysis.** Independent t test or one-way ANOVA test were used  
12 to analyze the experimental data. The values and error bars represent the mean values  
13 and standard deviations of three independent experiments, respectively. Statistical  
14 significance was expressed as \*\*p < 0.01 and \*p < 0.05.  
15  
16  
17  
18  
19  
20  
21

### 22 **3. RESULTS AND DISCUSSION**

23  
24  
25 **3.1. Preparation and characterization of CCM-CDs.** The optical properties of  
26 CCM-CDs was firstly characterized through UV-vis spectroscopy. In Figure 1a, the  
27 characteristic absorption peaks at about 282 nm and 225 nm should be attributed to  
28 n- $\pi^*$  and  $\pi$ - $\pi^*$  transition, respectively. The FL spectra showed that the maximum  
29 fluorescence emission wavelength was 460 nm, suggesting a blue light emission.  
30 Figure 1b showed the red shift of the emission wavelength of CCM-CDs from 460 to  
31 501 nm in the excitation wavelength range from 310 to 400 nm. This phenomenon  
32 was called the excitation-dependent FL behavior, which was thought to be connected  
33 with the distribution of different sizes and surface states of CCM-CDs.<sup>37</sup> Besides, the  
34 fluorescence spectra of CCM-CDs were detected after changing the time of pyrolysis.  
35 As displayed in Figure S1, the maximum fluorescence emission wavelength of the  
36 CCM-CDs had an obvious red shift with the increase of pyrolysis time, which was  
37 consistent with the conclusion of quantum confinement effects.<sup>38</sup> In Figure 1c, the  
38  
39  
40  
41  
42  
43  
44  
45  
46  
47  
48  
49  
50  
51  
52  
53  
54  
55  
56  
57  
58  
59  
60

1  
2  
3  
4 resulting CCM-CDs were uniform in size and spherical in shape. The lower right  
5  
6 corner of Figure 1c displayed the average size of CCM-CDs was  $1.5 \pm 0.3$  nm by  
7  
8 high-resolution TEM (HRTEM) calculation. The Gaussian fitting curve revealed that  
9  
10 the average diameters of CCM-CDs were 1.7 nm (Figure 1d) and the zeta potential of  
11  
12 CCM-CDs was  $15.6 \pm 2.05$  mV. Since the surface of the CCM-CDs was rich in  
13  
14 hydroxyl groups and the solution is slightly acidic (pH = 6.8). The hydroxyl groups  
15  
16 were hydration with the positively charged  $H_3O^+$  in the solution,<sup>39</sup> resulting in a  
17  
18 certain degree of positive charge on the surface of the CCM-CDs.  
19  
20  
21  
22  
23



46  
47  
48  
49  
50  
51  
52  
53  
54  
55  
56  
57  
58  
59  
60

**Figure 1.** (a) UV-vis absorption spectra and FL emission spectra of CCM-CDs in aqueous solution. (b) Excitation-dependent FL for CCM-CDs. (c) TEM and HRTEM images. Scale bar: 20 nm. (d) Size distribution of CCM-CDs.

The fluorescence lifetime of the CCM-CDs was evaluated through

1  
2  
3  
4 time-correlated single photon counting (Figure S2). The average lifetime  $\tau$  can be  
5  
6 calculated by the equation:  $\tau = (B_1\tau_1^2 + B_2\tau_2^2)/(B_1\tau + B_2\tau_2)$ .<sup>40</sup> Table S1 presented the  
7  
8 fitting parameters of  $\tau_1$ ,  $\tau_2$ ,  $B_1$ ,  $B_2$  and  $\tau$ , and the lifetime of the CCM-CDs was  $8.81 \pm$   
9  
10 1.25 ns. Taking the quinine sulfate (QY = 54%) as the standard, the quantum yield  
11  
12 (QY) of CCM-CDs was calculated to be 3.6% based on the previously reported  
13  
14 procedure.<sup>41,42</sup>  
15  
16  
17  
18

19 In Figure S3a, both curcumin and CCM-CDs showed different functional groups  
20  
21 except for the phenolic hydroxyl. The absorption band at  $3200-3400 \text{ cm}^{-1}$  was due to  
22  
23 the stretching vibration of phenolic hydroxyl groups, which appeared either in  
24  
25 curcumin or CCM-CDs. Phenolic hydroxyl groups in curcumin may play vital roles in  
26  
27 its anti-oxidant, anti-inflammatory and radical scavenging activities, implying the  
28  
29 potential vital roles of the phenolic hydroxyl groups in the antiviral activity of  
30  
31 CCM-CDs. Besides, the band observed at  $1622 \text{ cm}^{-1}$  in curcumin are due to C=O  
32  
33 vibration bands, which shifted to  $1650 \text{ cm}^{-1}$  in CCM-CDs. The peaks at 1217 and  
34  
35 1019  $\text{cm}^{-1}$  for curcumin explicitly demonstrated the exist of C-O-C and C-O, which  
36  
37 disappeared in CCM-CDs. In Figure S3b, the X-ray diffraction pattern demonstrated  
38  
39 the crystalline nature of the sample. Due to their nanoscale size, the diffraction peaks  
40  
41 of the CCM-CDs distinctly broadened, suggesting the existence of CDs. The  
42  
43 characteristic bands in the Raman spectra of CCM-CDs were located at around 1345  
44  
45 and 1595  $\text{cm}^{-1}$ , corresponding to the D band and G band, respectively (Figure  
46  
47 S3c).<sup>43,44</sup>  
48  
49  
50  
51  
52  
53  
54  
55

56 The overall XPS analysis of the CCM-CDs showed that there were two bands at  
57  
58  
59  
60

284.1 and 533.1 eV, corresponding to C 1s and O 1s (Figure 2a). The C 1s peaks at 284.6 and 288.8 eV (Figure 2b) attributed to the C-C and C=O functions, indicating that the synthetic CCM-CDs surface was rich in hydrophilic groups.<sup>7</sup> A contribution at 531.8 and 533.0 eV of O 1s showed due to the C=O and C-OH/C-O-C functions (Figure 2c).<sup>45</sup> The surface composition of the CCM-CDs as determined by XPS was accordance with the corresponding FT-IR conclusion. These results indicated that the remaining curcumin and citrate are not carbonized and remained on the surface of carbon dots as protective groups.

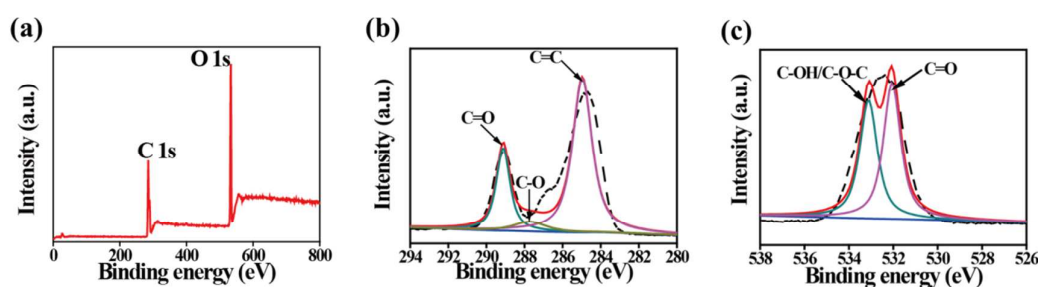
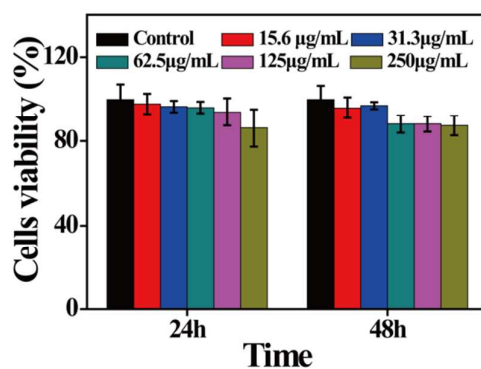


**Figure 2.** XPS-survey spectra of CCM-CDs derived from curcumin. Overall spectrum (a), C 1s (b) and O 1s (c) high-resolution survey spectra of the CCM-CDs.

**3.2. Toxicity of CCM-CDs on cells.** *In vitro* cytotoxicity of CCM-CDs against Vero cells and PK-15 cells was evaluated via CCK-8 assay (Figure 3 and Figure S4). As presented in Figure 3, the survival rate of Vero cells exposed with various concentrations of CCM-CDs for a different incubation time (24 and 48 h). As expected, Vero cells were co-incubated with CCM-CDs concentration ranges from 15.6 to 125  $\mu\text{g/mL}$  *in vitro* and cell viability was observed to exceed 90% after 24 and 48 h, confirming the low cytotoxicity of the as-prepared CCM-CDs. To test whether

1  
2  
3  
4 DMSO had an effect on the stability of CCM-CDs at low concentrations, the particle  
5  
6 size of CCM-CDs in DMSO was measured. The average hydrodynamic size was 1.6  
7  
8 nm (Figure S5). This was close to the size measured when the solvent was water,  
9  
10 indicating that the effect of DMSO on CCM-CDs could be ignored. Thus, 125  $\mu\text{g}/\text{mL}$   
11  
12 CCM-CDs were used for the following antiviral experiments.  
13  
14  
15  
16  
17



18  
19  
20  
21  
22  
23  
24  
25  
26  
27  
28  
29  
30  
31 **Figure 3.** The effects of different concentrations of CCM-CDs on Vero cells viability  
32  
33 were detected by CCK-8 assay.  
34  
35

36  
37 **3.3. Antiviral activity of CCM-CDs against PEDV infection.** The inhibitory  
38  
39 effect of the CCM-CDs was investigated through one-step growth curve assay to  
40  
41 evaluate the infectivity of PEDV. Specifically, the replication of PEDV in Vero cells  
42  
43 was determined with treatment and untreated of 125  $\mu\text{g}/\text{mL}$  CCM-CDs, followed  
44  
45 by quantifying of viral titers. As displayed in Figure 4a, compared with the control  
46  
47 groups, the virus titer of the experimental groups were obviously reduced,  
48  
49 demonstrating the efficient inhibitory effect of the CCM-CDs on PEDV infection.  
50  
51 Meanwhile, it can be visually observed that the plaque numbers were distinctly  
52  
53 reduced when exposure with CCM-CDs (Figure 4b). The reduction of plaque numbers  
54  
55  
56  
57  
58  
59  
60

and decrease of virus titers indicated that CCM-CDs can effectively inhibit virus replication.

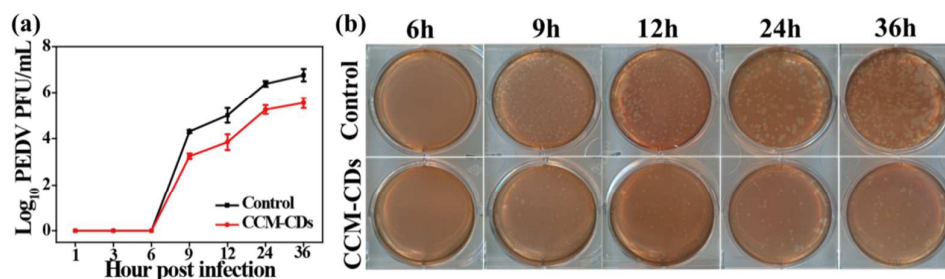


**Figure 4.** One-step growth curves of virus in the absence and presence of CCM-CDs

(a). Virus titers were detected in the presence and absence of CCM-CDs and photos were taken after 2-3 days post infection (b).

The protective effects of CCM-CDs were detected by fluorescent inverted microscopy. In Figure S6a, no cytopathic effect (CPE) was noticed in the negative control group. Cells treated with PEDV showed lysis and detachment from the cell monolayer at 12 hours post infection (hpi) (Figure S6b). However, the cytopathic effect was gradually diminished when treated with different concentrations of CCM-CDs (Figure S6c and S6d). These results suggested that CCM-CDs interfered with the infectivity of PEDV.

To study the inhibitory effect of CCM-CDs, the expression of PEDV N proteins in Vero cells was detected. In Figure 5a, the green fluorescence signals of the experimental groups were dramatically reduced, which is directly reflected in the decrease of the expression level of PEDV N protein. These results were confirmed by western blot analysis (Figure 5b). To test whether the quenching effect of carbon dots

will influence the fluorescence, the fluorescence image was observed by using a confocal laser-scanning microscope. A weak blue fluorescence can be observed, indicating that CCM-CDs can be taken by Vero cell (Figure S7). However, the fluorescence of CCM-CDs can be neglected in comparison with that of FITC and DAPI. These results excluded the probability that the aforementioned reduction of viral titers was resulted from cellular toxicity of the CCM-CDs.

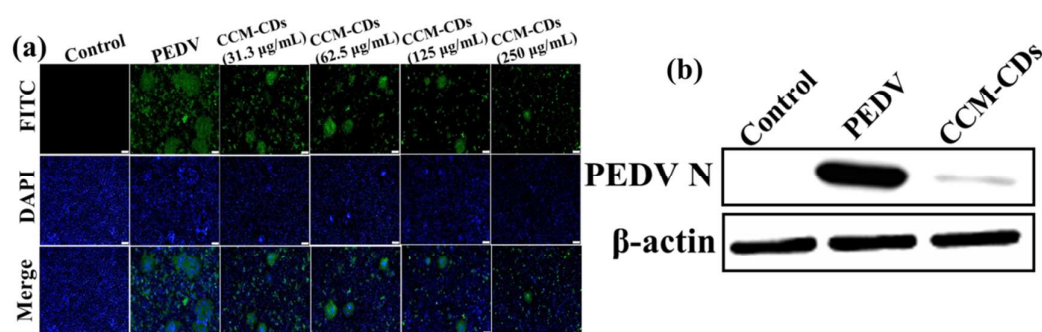


**Figure 5.** The effect of CCM-CDs on PEDV. (a) The effect of different concentrations of CCM-CDs on PEDV-infected Vero cells by indirect immunofluorescence assay. Scale bar: 100 µm. (b) The expression level of PEDV N protein in the presence of 125 µg/mL CCM-CDs at 12 hpi by western blot analysis.

The antiviral activity of CCM-CDs was also compared to that of EDA-CDs as ethylenediamine (EDA) is a common surface passivation reagent for the preparation of high yield CDs.<sup>31</sup> The optical properties and surface functional groups of the EDA-CDs were displayed in Figure S8. In Figure 6a, EDA-CDs were found almost impossible to suppress the virus infection at all tested concentrations. In Figure 6b and 6c, the virus titer values and plaque numbers revealed that CCM-CDs had a superior antiviral effect to EDA-CDs. The CCM-CDs showed a higher zeta potential (+15.6

mV) than EDA-CDs (-5.1 mV). Moreover, the effect of a positively charged CDs (33 mV) on PEDV N protein was also analyzed by western blot. From the Figure S9, it can be seen that the positively charged CDs showed a decrease in PEDV N protein expression than that of the control groups. We speculate that the surface charge of the CCM-CDs plays a small part in their antiviral efficacy. The positively charged CCM-CD on the surface undergoes strong electrostatic interactions with PEDV or cell membranes, thereby competing to bind the virus to cells.

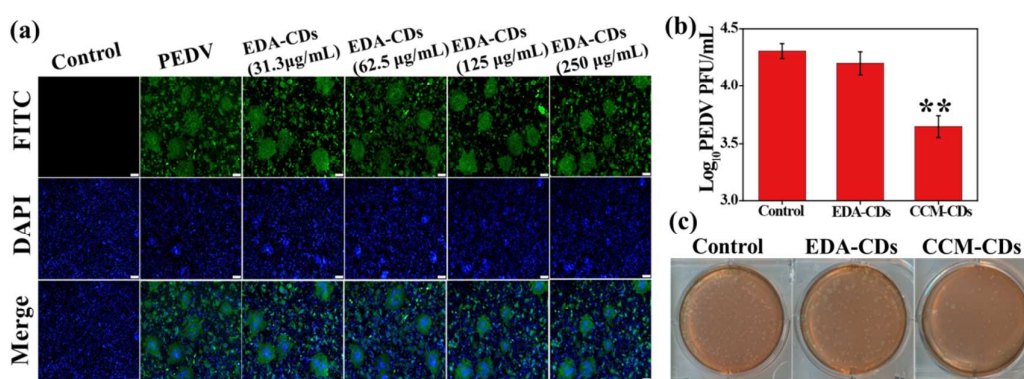


**Figure 6.** The effect of EDA-CDs on PEDV. (a) The effect of different concentrations of EDA-CDs on PEDV-infected Vero cells by indirect immunofluorescence assay. Scale bar: 100 µm. (b) The titer of PEDV when exposed or unexposed to 125 µg/mL EDA-CDs or CCM-CDs. All error bars were determined according to the three replicate experiments. (c) Virus titers were calculated in the presence and absence of EDA-CDs or CCM-CDs. Pictures were taken at 12 hpi.

**3.4. Mechanism of viral inhibition.** The proposed antiviral mechanisms of CCM-CDs cover direct action on viral entry, penetration, replication and budding.<sup>46</sup> And thus a set of experiments were carried out to identify which stage(s) of the viral

1  
2  
3  
4 life cycle were suppressed by CCM-CDs.  
5  
6

7 The influence of CCM-CDs on virus entry was evaluated by using plaque  
8 reduction analysis. PEDV samples were first treated with different concentrations of  
9 CCM-CDs, then inoculated into the cells (37 °C/1 h). In Figure 7a, CCM-CDs  
10 showed a strong concentration-dependent inhibitory effect on PEDV, suggesting that  
11 they blocked PEDV infection at the early stages of viral entry. The inhibition  
12 efficiency of CCM-CDs (125 µg/mL) on virus entry was over 50%. Furthermore, the  
13 zeta potentials of CCM-CDs, PEDV and CCM-CDs pretreated with PEDV were  
14 measured, and they were +15.6, -6.42 and -0.18 mV, respectively (Figure 7b),  
15 implying that the positively charged CCM-CDs may cause virus aggregation through  
16 electrostatic interaction, resulting in reduced viral infectivity. These results were  
17 verified through fluorescence and Raman spectral analysis. Figure 7c showed that the  
18 fluorescence intensity and the maximum emission of CCM-CDs decreased gradually  
19 and exhibited an apparent red shift along with the increase of PEDV concentration,  
20 indicating the occurrence of interaction between CCM-CDs and PEDV.<sup>47</sup> To  
21 demonstrate the interaction between CCM-CDs and PEDV, Raman displacement tests  
22 were carried out for PEDV when it was exposed or unexposed to different  
23 concentrations of CCM-CDs. From Figure 7d, it can be seen that, with the amount of  
24 CCM-CDs increasing, the Raman spectra exhibited most obvious differences in the  
25 shifts of 333, 457, 521, 597, 777, 828, 920, 1123, 1313 and 1447 cm<sup>-1</sup>. The peaks at  
26 521 and 777 cm<sup>-1</sup> were attributed to S-S disulfide stretch in proteins and  
27 cytosine/uracil ring breathing, respectively.<sup>48</sup> The peak at 828 cm<sup>-1</sup> was assigned to  
28  
29  
30  
31  
32  
33  
34  
35  
36  
37  
38  
39  
40  
41  
42  
43  
44  
45  
46  
47  
48  
49  
50  
51  
52  
53  
54  
55  
56  
57  
58  
59  
60

the out-of-plane ring breathing tyrosine. The bands at 920, 1123, 1313 and 1447  $\text{cm}^{-1}$  corresponded to C-C stretch of proline ring, C-C stretching mode of lipids/protein,  $\text{CH}_3\text{CH}_2$  twisting mode of collagen/lipids and  $\text{CH}_2$  bending mode of proteins and lipids.<sup>49,50</sup> These observation suggested that the addition of CCM-CDs had changed the structure of the protein.

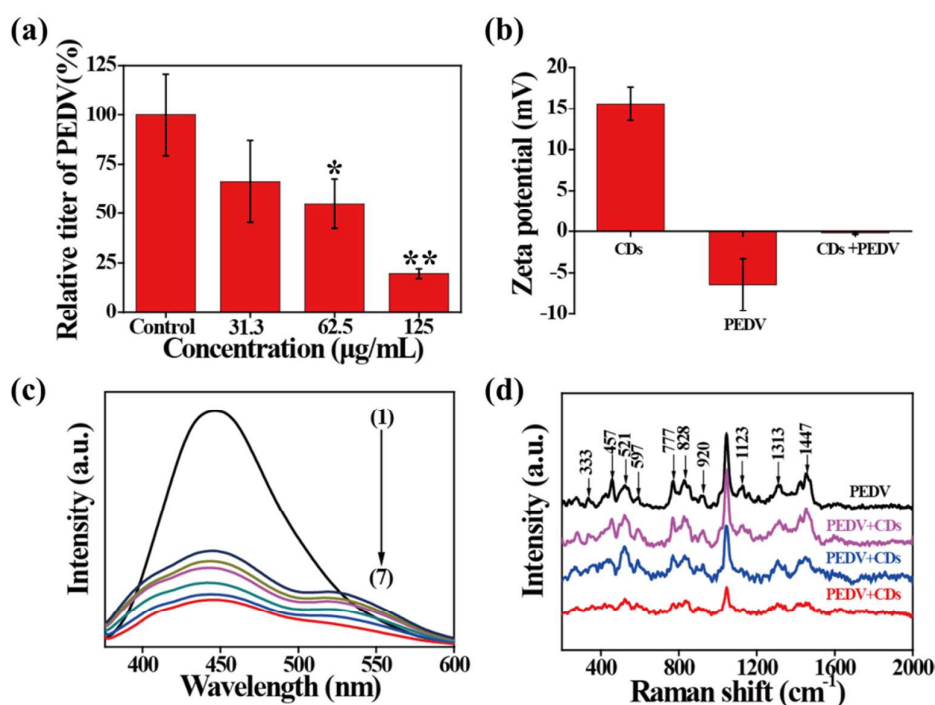


**Figure 7.** (a) The dose relationship between the viral entry inhibitory efficiency and the amount of CCM-CDs added. (b) The zeta potentials of the CCM-CDs, PEDV and CCM-CDs pretreated with PEDV, respectively. (c) Fluorescence spectra of CCM-CDs. CCM-CDs (125  $\mu\text{g/mL}$ ) were exposed to PEDV (1-7: 0,  $1 \times 10^5$ ,  $2 \times 10^5$ ,  $3 \times 10^5$ ,  $4 \times 10^5$ ,  $5 \times 10^5$ ,  $6 \times 10^5$  PFU/mL). (d) Raman spectral analysis of PEDV and CCM-CDs-treated PEDV. Black line is PEDV ( $10^5$  PFU/mL), pink line represents PEDV ( $10^5$  PFU/mL) pretreated with 31.3  $\mu\text{g/mL}$  CCM-CDs, blue line represents PEDV ( $10^5$  PFU/mL) pretreated with 62.5  $\mu\text{g/mL}$  CCM-CDs and red line indicates

PEDV ( $10^5$  PFU/mL) pretreated with 125  $\mu\text{g/mL}$  CCM-CDs, respectively.

In order to test whether CCM-CDs can inhibit viral penetration, different concentrations of CCM-CDs were injected after attaching PEDV to the cell surface ( $4\text{ }^\circ\text{C}/2\text{ h}$ ), then penetration was started through transferring temperature to  $37\text{ }^\circ\text{C}$ . In Figure 8a, no noticeable difference was observed from viral titers after treatment or untreated with CCM-CDs, indicating that the CCM-CDs did not inhibit viral penetration. It is well documented that the synthesis of PEDV negative-strand RNA begins soon after penetrating into the infected cells. The inhibitory activity of CCM-CDs on negative-strand RNA synthesis was evaluated. The negative-strand RNA level of PEDV showed a remarkable down-regulation in CCM-CDs-treated cells compared to the untreated control at different hours post infection, suggesting that CCM-CDs can effectively inhibit PEDV at the replication step (Figure 8b).

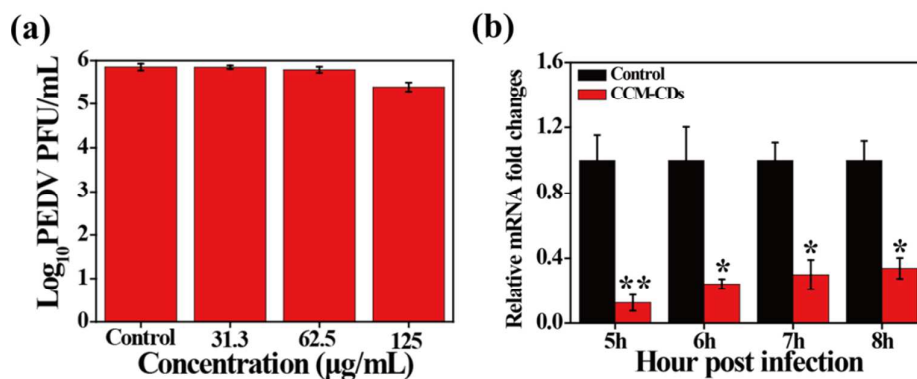


**Figure 8.** (a) The dose relationship between the viral entry inhibitory efficiency and the amount of CCM-CDs used. (b) The relative synthesis of PEDV negative-strand RNA was measured after infection for various times.

To probe the influence of CCM-CDs on virion budding, viral titers in the

intracellular and supernatant after various times of CCM-CDs treatment were quantified. In Figure 9a, significant differences were detected in PEDV intracellular titers between CCM-CDs-treatment groups and the control groups. Whereas, the virus titer in the supernatant treated with CCM-CDs was only slightly less those in the control group, indicating that CCM-CDs could inhibit viral budding (Figure 9b).

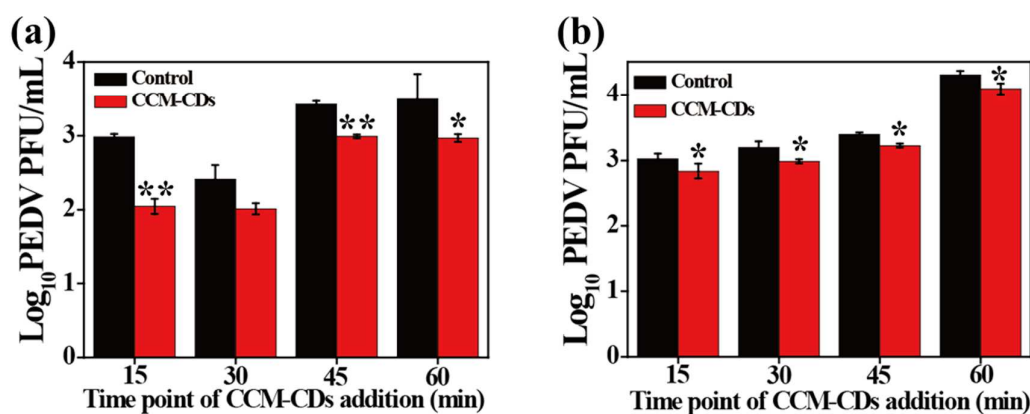


**Figure 9.** The titer of PEDV was quantified after treatment with CCM-CDs at different time points. Viral titer in intracellular (a) and in supernatant (b).

**3.5. CCM-CDs activation of antiviral innate immunity.** Innate immune response offers the first defense line against the invasion of pathogens and limits their spread.<sup>51,52</sup> Incoming viruses can activate nuclear factor- $\kappa$ B (NF- $\kappa$ B) and/or interferon-regulatory factors (IRFs) to induce the expression of hundreds of antiviral cytokines, including interferons (IFNs) and proinflammatory cytokines. Antiviral IFNs signal via the JAK/STAT pathway to drive the synthesis of a great number of IFN-stimulated genes (ISGs) or through direct stimulation in an IFN-independent pathway to collaboratively stop different stages of viral replication during viral replication cycle.<sup>53</sup> To investigate whether CCM-CDs can trigger host innate immune

1  
2  
3  
4 response, we examined the influence of CCM-CDs on the expressions of ISGs and  
5  
6 proinflammatory cytokines in vitro by measuring their mRNA levels using RT-PCR  
7  
8 (Figure S10 and S11). After CCM-CDs treatment, an obviously up-regulated  
9  
10 expression could be observed in interferon inducible protein 10 (IP-10) (Figure S10a),  
11  
12 interferon stimulated gene 54 (ISG-54) (Figure S10b), MxA (Figure S10c) and  
13  
14 interferon stimulated gene 20 (ISG-20) (Figure S10f). The mRNA expression levels of  
15  
16 interleukin 8 (IL-8) (Figure S10d) and interleukin 6 (IL-6) (Figure S10e) were also  
17  
18 5.8- and 3.0-fold more in cells treated with CCM-CDs than in the untreated controls.  
19  
20  
21  
22  
23 It was found that TRIM32 can be used as an antiviral factor mainly by activating the  
24  
25 interferon immune response and promoting the expression of IL-8 and IL-6.<sup>54</sup> This  
26  
27 was consistent with our conclusion.  
28  
29  
30

31  
32 The cooperativity of the transcription factors IRF3 and NF- $\kappa$ B are necessary for  
33  
34 the induction of ISGs and pro-inflammatory cytokines. To examine whether  
35  
36 CCM-CDs induced expression of IRF-3 and NF- $\kappa$ B, Vero cells were first exposed or  
37  
38 unexposed with CCM-CDs, then the IRF3-Luc, NF- $\kappa$ B-Luc luciferase reporter  
39  
40 plasmids and the internal control plasmid pRL-TK were co-transfected. As  
41  
42 demonstrated in Figure 10a and 10b, the CCM-CDs could upregulate IRF3 and  
43  
44 NF- $\kappa$ B promoter activity. Moreover, the production of phosphorylated IRF3 (p-IRF3)  
45  
46 and p65 (p-p65) proteins in CCM-CDs treatment group was dramatically higher than  
47  
48 that in control group (Figure 10c and 10d). The phosphorylation of IRF3 and NF- $\kappa$ B  
49  
50 subunit p65 was considered to be the sign of IRF3 and NF- $\kappa$ B. Collectively, all these  
51  
52 data revealed that innate immune response might be triggered in vitro by the  
53  
54  
55  
56  
57  
58  
59  
60

CCM-CDs treatment.

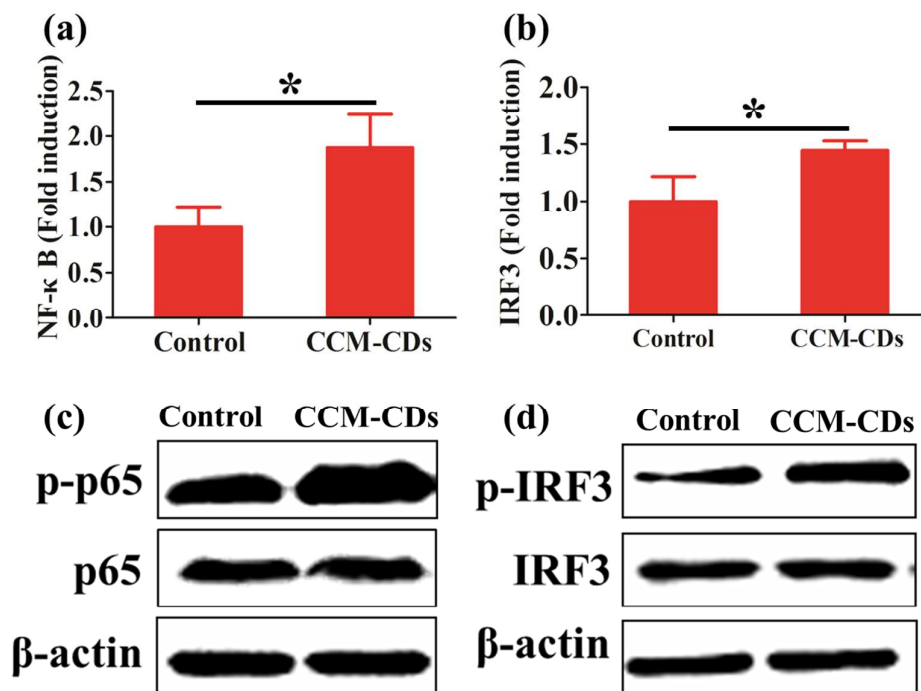


**Figure 10.** CCM-CDs upregulated the expression of IRF3 and NF-κB promoter. Cells were cotransfected with the NF-κB-Luc (a) and IRF3-Luc (b) together with the pRL-TK plasmid. When exposure with CCM-CDs for 12 h, the luciferase test was carried out. CCM-CDs treatment stimulated phosphorylation of IRF3 and p65 (c, d). Cells were treated with CCM-CDs for 12 h, and then cells were harvested and detected by western blot assays with specific antibodies.

**3.6. Inhibition on ROS generation by CCM-CDs.** The infection of certain viruses occurs simultaneously with the overexpression of reactive oxygen species (ROS), leading to DNA damage by regulating apoptotic signaling pathways. In order to probe whether CCM-CDs can suppress ROS generation, 2',7'-dichlorodihydrofluorescein diacetate (DCFH-DA) test was performed. The

1  
2  
3 stronger fluorescent intensity of DCF was observed in PEDV-infected cells compared  
4  
5  
6 to the control group (Figure S12a and S12b). However, after treatment with  
7  
8 CCM-CDs, the fluorescence intensity turned weak (Figure S12c). Since most  
9  
10 curcumin was carbonized at high temperatures, and the prepared CCM-CDs was  
11  
12 centrifuged and dialyzed to remove unreacted small molecules. And the presence of  
13  
14 free curcumin was excluded, which indicated that CCM-CDs could inhibit ROS  
15  
16 generation induced by PEDV infection..  
17  
18  
19  
20

#### 21 **4. CONCLUSION**

22  
23  
24 In conclusion, the fluorescent CCM-CDs were obtained by a simple one-step method  
25  
26 of pyrolysis of curcumin and its detailed characterization was performed. The  
27  
28 characterization results showed that the CCM-CDs had an ultrasmall size (diameter *ca.*  
29  
30 1.5 nm ), rich hydrophilic groups and a positive potential (+ 15.6 mV).  
31  
32  
33  
34

35 This is the first report showing that CCM-CDs obtained by pyrolysis of herbs  
36  
37 have prominent antiviral activity against PEDV infection. Compared with the  
38  
39 common CDs synthesized by pyrolysis of ethylenediamine, the cationic CCM-CDs  
40  
41 possess better antiviral properties. The underlying mechanism analysis indicates that  
42  
43 CCM-CDs exposure can inhibit the viral entry through changing the structure of viral  
44  
45 surface protein, and prevent the synthesis and budding of negative-strand RNA in  
46  
47 virus. It has also been demonstrated that CCM-CDs could obviously suppress the  
48  
49 accumulation of ROS caused by the PEDV. Furthermore, CCM-CDs treatment can  
50  
51 suppress virus reproduction by activating the production of interferon-stimulating  
52  
53  
54  
55  
56  
57  
58  
59  
60

1  
2  
3 genes (ISGs) and pro-inflammatory cytokines of Vero cells.  
4  
5

6  
7 Our results provide a novel clue to improve the antiviral activity of herbs. The  
8  
9 integrated data indicate that CCM-CDs can be potentially applied against not only  
10  
11 PEDV but also other viruses. However, further evaluation needs to be performed on  
12  
13 the prophylactic and therapeutic effects of CCM-CDs using an appropriate animal  
14  
15 model.  
16  
17  
18

## 19 20 **ASSOCIATED CONTENT**

### 21 22 **Supporting Information**

23  
24  
25  
26 Supplementary data including: synthesis routes of CCM-CDs (Scheme S1),  
27  
28 fluorescent spectra (Figure S1), fluorescence decay curves (Figure S2 and Table S1),  
29  
30 primers sequence (Table S2), FTIR spectra, Raman spectra and XRD patterns of  
31  
32 CCM-CDs (Figure S3), cytopathic of Vero cells (Figure S4), size distribution (Figure  
33  
34 S5), cytopathic effects of Vero cells (Figure S6), fluorescence microscopy images  
35  
36 (Figure S7), characterization of EDA-CDs (Figure S8), western blot (Figure S9),  
37  
38 real-time RT-PCR assay (Figure S10 and S11) and indirect immunofluorescence assay  
39  
40 (Figure S12) .  
41  
42  
43  
44  
45

## 46 47 **AUTHOR INFORMATION**

### 48 49 **Corresponding Authors**

50  
51  
52  
53 \*E-mail: hyhan@mail.hzau.edu.cn;  
54  
55

56 \*E-mail: vet@mail.hzau.edu.cn.  
57  
58  
59  
60

1  
2  
3 \*These authors jointly supervised this work.  
4  
5

6  
7 **Notes**  
8

9  
10 The authors declare no competing financial interest.  
11  
12

13 **ACKNOWLEDGMENTS**  
14

15  
16 This research was supported by the National Key R & D Program  
17 (2016YFD0500700) and the National Natural Science Foundation of China  
18 (21375043, 21778020, 31672569, 31402239) and Sci-tech Innovation Foundation of  
19 Huazhong Agriculture University (2662017PY042).  
20  
21  
22  
23  
24  
25

26  
27 **REFERENCES**  
28

- 29  
30 (1) Lv, Y. L.; Gong, L. L.; Wang, Z. H.; Han, F. F.; Liu, H.; Lu, X. C.; Liu, L. H.  
31  
32 Curcumin Inhibits Human Cytomegalovirus by Downregulating Heat Shock  
33 Protein 90. *Mol. Med. Rep.* **2015**, *12*, 4789-4793.  
34  
35  
36  
37  
38 (2) Teymouri, M.; Pirro, M.; Johnston, T. P.; Sahebkar, A. Curcumin as a Multifaceted  
39  
40 Compound against Human Papilloma Virus Infection and Cervical Cancers: A  
41 Review of Chemistry, Cellular, Molecular, and Preclinical Features. *BioFactors*  
42  
43 **2017**, *43*, 331-346.  
44  
45  
46  
47  
48 (3) Zheng, M.; Liu, S.; Guan, X. G.; Xie, Z. G. One-Step Synthesis of Nanoscale  
49  
50 Zeolitic Imidazolate Frameworks with High Curcumin Loading for Treatment of  
51  
52 Cervical Cancer. *ACS Appl. Mater. Interfaces* **2015**, *7*, 22181-22187.  
53  
54  
55  
56  
57  
58  
59  
60

- 1  
2  
3  
4 (4) Mouler Rechtman, M.; Har Noy O.; Bar Yishay I.; Fishman, S.; Adamovich, Y.;  
5  
6 Shaul, Y.; Halpern, Z.; Shlomain, A. Curcumin Inhibits Hepatitis B Virus via  
7  
8 Down-Regulation of the Metabolic Coactivator PGC-1 $\alpha$ . *FEBS Lett.* **2010**, *584*,  
9  
10 2485-2490.  
11  
12  
13  
14 (5) Ali, A.; Banerjea, A. C. Curcumin Inhibits HIV-1 by Promoting Tat Protein  
15  
16 Degradation. *Sci. Rep.* **2016**, *6*, 27539-27548.  
17  
18  
19  
20 (6) Narayanan, A.; Kehn Hall, K.; Senina, S.; Lundberg, L.; Van Duyne, R.; Guendel,  
21  
22 I.; Das, R.; Baer, A.; Bethel, L.; Turell, M.; Hartman, A. L.; Das, B.; Bailey, C.;  
23  
24 Kashanchi, F. Curcumin Inhibits Rift Valley Fever Virus Replication in Human  
25  
26 Cells. *J. Biol. Chem.* **2012**, *287*, 33198-33214.  
27  
28  
29  
30 (7) Yang, X. X.; Li, C. M.; Huang, C. Z. Curcumin Modified Silver Nanoparticles for  
31  
32 Highly Efficient Inhibition of Respiratory Syncytial Virus Infection. *Nanoscale*  
33  
34 **2016**, *8*, 3040-3048.  
35  
36  
37  
38 (8) Yang, X. X.; Li, C. M.; Li, Y. F.; Wang, J.; Huang, C. Z. Synergistic Antiviral  
39  
40 Effect of Curcumin Functionalized Graphene Oxide against Respiratory Syncytial  
41  
42 Virus Infection. *Nanoscale* **2017**, *9*, 16086-16092.  
43  
44  
45  
46 (9) Lembo, D.; Cavalli, R. Nanoparticulate Delivery Systems for Antiviral Drugs.  
47  
48 *Antivir. Chem. Chemoth.* **2010**, *21*, 53-70.  
49  
50  
51  
52 (10) Szunerits, S.; Barras, A.; Khanal, M.; Pagneux, Q.; Boukherroub, R.  
53  
54 Nanostructures for the Inhibition of Viral Infections. *Molecules* **2015**, *20*,  
55  
56  
57  
58  
59  
60

1  
2  
3  
4 14051-14081.  
5

6  
7 (11) Yadavalli, T.; Shukla, D. Role of Metal and Metal Oxide Nanoparticles as  
8  
9 Diagnostic and Therapeutic Tools for Highly Prevalent Viral Infections.  
10  
11 *Nanomed. Nanotechnol.* **2017**, *13*, 219-230.  
12

13  
14  
15 (12) Singh, L.; Kruger, H. G.; Maguire, G. E. M.; Govender, T.; Parboosing, R. The  
16  
17 Role of Nanotechnology in the Treatment of Viral Infections. *Ther. Adv. Infect. Dis.*  
18  
19 **2017**, *4*, 105-131.  
20  
21

22  
23 (13) Draz, M. S.; Wang, Y. J.; Chen, F. F.; Xu, Y. H.; Shafiee, H. Electrically  
24  
25 Oscillating Plasmonic Nanoparticles for Enhanced DNA Vaccination against  
26  
27 Hepatitis C Virus. *Adv. Funct. Mater.* **2017**, *27*, 1604139-1604149.  
28  
29

30  
31 (14) Vonnemann, J.; Sieben, C.; Wolff, C.; Ludwig, K.; Bottcher, C.; Herrmann, A.;  
32  
33 Haag, R. Virus Inhibition Induced by Polyvalent Nanoparticles of Different Sizes.  
34  
35 *Nanoscale* **2014**, *6*, 2353-2360.  
36  
37

38  
39 (15) Li, L.; Fu, F.; Xue, M.; Chen, W.; Liu, J.; Shi, H.; Chen, J.; Bu, Z.; Feng, L.; Liu,  
40  
41 P. IFN-Lambda Preferably Inhibits PEDV Infection of Porcine Intestinal  
42  
43 Epithelial Cells Compared with IFN-Alpha. *Antivir. Res.* **2017**, *140*, 76-82.  
44  
45

46  
47 (16) Bhatia, S.; Lauster, D.; Bardua, M.; Ludwig, K.; Angioletti-Uberti, S.; Popp, N.;  
48  
49 Hoffmann, U.; Paulus, F.; Budt, M.; Stadtmuller, M.; Wolff, T.; Hamann, A.;  
50  
51 Bottcher, C.; Herrmann, A.; Haag, R. Linear Polysialoside Outperforms  
52  
53 Dendritic Analogs for Inhibition of Influenza Virus Infection in Vitro and in Vivo.  
54  
55  
56  
57  
58  
59  
60

1  
2  
3  
4  
5  
6  
7  
8  
9  
10  
11  
12  
13  
14  
15  
16  
17  
18  
19  
20  
21  
22  
23  
24  
25  
26  
27  
28  
29  
30  
31  
32  
33  
34  
35  
36  
37  
38  
39  
40  
41  
42  
43  
44  
45  
46  
47  
48  
49  
50  
51  
52  
53  
54  
55  
56  
57  
58  
59  
60

*Biomaterials* **2017**, *138*, 22-34.

(17) Ziem, B.; Azab, W.; Gholami, M. F.; Rabe, J. P.; Osterrieder, N.; Haag, R. Size-Dependent Inhibition of Herpesvirus Cellular Entry by Polyvalent Nanoarchitectures. *Nanoscale* **2017**, *9*, 3774-3783.

(18) Ziem, B.; Rahn, J.; Donskyi, I.; Silberreis, K.; Cuellar, L.; Dervede, J.; Keil, G.; Mettenleiter, T. C.; Haag, R. Polyvalent 2D Entry Inhibitors for Pseudorabies and African Swine Fever Virus. *Macromol. Biosci.* **2017**, *17*, 3774-3783.

(19) Kwon, S. J.; Na, D. H.; Kwak, J. H.; Douaisi, M.; Zhang, F.; Park, E. J.; Park, J. H.; Youn, H.; Song, C. S.; Kane, R. S.; Dordick, J. S.; Lee, K. B.; Linhardt, R. J. Nanostructured Glycan Architecture is Important in the Inhibition of Influenza A Virus Infection. *Nat. Nanotechnol.* **2017**, *12*, 48-54.

(20) Castro-Mayorga, J. L.; Randazzo, W.; Fabra, M. J.; Lagaron, J. M.; Aznar, R.; Sánchez, G. Antiviral Properties of Silver Nanoparticles against Norovirus Surrogates and Their Efficacy in Coated Polyhydroxyalkanoates Systems. *LWT Food Sci. Technol.* **2017**, *79*, 503-510.

(21) Lv, X.; Wang, P.; Bai, R.; Cong, Y.; Suo, S.; Ren, X.; Chen, C. Inhibitory Effect of Silver Nanomaterials on Transmissible Virus-Induced Host Cell Infections. *Biomaterials* **2014**, *35*, 4195-4203.

(22) Akbarzadeh, A.; Kafshdooz, L.; Razban, Z.; Dastranj Tbrizi, A.; Rasoulpour, S.; Khalilov, R.; Kavetsky, T.; Saghfi, S.; Nasibova, A. N.; Kaamyabi, S.;

- 1  
2  
3 Kafshdooz, T. An Overview Application of Silver Nanoparticles in Inhibition of  
4 Herpes Simplex Virus. *Artif. Cell. Nanomed. Biotechnol.* **2018**, *46*, 236-267.  
5  
6  
7  
8  
9 (23) Nagy, A.; Steinbrück, A.; Gao, J.; Doggett, N.; Hollingsworth, J. A.; Iyer, R.  
10 Comprehensive Analysis of the Effects of CdSe Quantum Dot Size, Surface  
11 Charge, and Functionalization on Primary Human Lung Cells. *ACS Nano* **2012**, *6*,  
12 4748-4762.  
13  
14  
15  
16  
17  
18  
19 (24) Liu, X.; Huang, N.; Li, H.; Jin, Q.; Ji, J. Surface and Size Effects on Cell  
20 Interaction of Gold Nanoparticles with both Phagocytic and Nonphagocytic Cells.  
21 *Langmuir* **2013**, *29*, 9138-9148.  
22  
23  
24  
25  
26  
27  
28 (25) Deokar, A. R.; Nagvenkar, A. P.; Kalt, I.; Shani, L.; Yeshurun, Y.; Gedanken, A.;  
29 Sarid, R. Graphene-Based "Hot Plate" for the Capture and Destruction of the  
30 Herpes Simplex Virus Type 1. *Bioconjugate Chem.* **2017**, *28*, 1115-1122.  
31  
32  
33  
34  
35  
36 (26) Barras, A.; Pagneux, Q.; Sane, F.; Wang, Q.; Boukherroub, R.; Hober, D.;  
37 Szunerits, S. High Efficiency of Functional Carbon Nanodots as Entry Inhibitors  
38 of Herpes Simplex Virus Type 1. *ACS Appl. Mater. Interfaces* **2016**, *8*,  
39 9004-9013.  
40  
41  
42  
43  
44  
45  
46 (27) Y. Liu, B. Yan, D. A. Winkler, J. Fu, A. Zhang. Competitive Inhibition  
47 Mechanism of Acetylcholinesterase without Catalytic Active Site Interaction:  
48 Study on Functionalized C60 Nanoparticles via in Vitro and in Silico Assays.  
49 *ACS Appl. Mater. Interfaces* **2017**, *9*, 18626-18638.  
50  
51  
52  
53  
54  
55  
56  
57  
58  
59  
60

- 1  
2  
3  
4 (28) Sametband, M.; Kalt, I.; Gedanken, A.; Sarid, R. Herpes Simplex Virus Type-1  
5  
6 Attachment Inhibition by Functionalized Graphene Oxide. *ACS Appl. Mater.*  
7  
8 *Interfaces* **2014**, *6*, 1228-1235.  
9  
10  
11 (29) Du, T.; Liang, J. G.; Dong, N.; Liu, L.; Fang, L. R.; Xiao, S. B.; Han, H. Y.  
12  
13 Carbon Dots as Inhibitors of Virus by Activation of Type I Interferon Response.  
14  
15 *Carbon* **2016**, *110*, 278-285.  
16  
17  
18  
19 (30) Zhang, H.; Chen, Y.; Liang, M.; Xu, L.; Qi, S.; Chen, H.; Chen, X. Solid-Phase  
20  
21 Synthesis of Highly Fluorescent Nitrogen-Doped Carbon Dots for Sensitive and  
22  
23 Selective Probing Ferric Ions in Living Cells. *Anal. Chem.* **2014**, *86*, 9846-9852.  
24  
25  
26  
27 (31) Li, F.; Liu, C.; Yang, J.; Wang, Z.; Liu, W.; Tian, F. Mg/N Double Doping  
28  
29 Strategy to Fabricate Extremely High Luminescent Carbon Dots for Bioimaging.  
30  
31 *RSC Adv.* **2014**, *4*, 3201-3205.  
32  
33  
34  
35 (32) Yang, S. T.; Wang, X.; Wang, H.; Lu, F.; Luo, P. G.; Cao, L.; Mezziani, M. J.; Liu,  
36  
37 J. H.; Liu, Y.; Chen, M. Carbon Dots as Nontoxic and High-Performance  
38  
39 Fluorescence Imaging Agents. *J. Phys. Chem. C* **2009**, *113*, 18110-18114.  
40  
41  
42  
43 (33) Alvarez, A. L.; Melon, S.; Dalton, K. P.; Nicieza, I.; Roque, A.; Suarez, B.; Parra,  
44  
45 F. Apple Pomace, a by-Product from the Asturian Cider Industry, Inhibits Herpes  
46  
47 Simplex Virus Types 1 and 2 in Vitro Replication: Study of its Mechanisms of  
48  
49 Action. *J. Med. Food* **2012**, *15*, 581-587.  
50  
51  
52  
53 (34) Gescher, K.; Hensel, A.; Hafezi, W.; Derksen, A.; Kühn, J. Oligomeric  
54  
55  
56  
57  
58  
59  
60

- 1  
2  
3 Proanthocyanidins from *Rumex Acetosa* L. Inhibit the Attachment of Herpes  
4  
5 Simplex Virus Type-1. *Antivir. Res.* **2011**, *89*, 9-18.  
6  
7  
8  
9 (35) Duan, E.; Wang, D.; Fang, L.; Ma, J.; Luo, J.; Chen, H.; Li, K.; Xiao, S.  
10  
11 Suppression of Porcine Reproductive and Respiratory Syndrome Virus  
12  
13 Proliferation by Glycyrrhizin. *Antivir. Res.* **2015**, *120*, 122-125.  
14  
15  
16  
17 (36) Li, Y. H.; Lin, Z. F.; Zhao, M. Q.; Xu, T. T.; Wang, C. B.; Hua, L.; Wang, H. Z.;  
18  
19 Xia, H. M.; Zhu, B. Silver Nanoparticle Based Codelivery of Oseltamivir to  
20  
21 Inhibit the Activity of the H1N1 Influenza Virus through ROS-Mediated  
22  
23 Signaling Pathways. *ACS Appl. Mater. Interfaces* **2016**, *8*, 24385-24393.  
24  
25  
26  
27 (37) Gao, T.; Wang, X.; Yang, L. Y.; He, H.; Ba, X. X.; Zhao, J.; Jiang, F. L.; Liu, Y.  
28  
29 Red, Yellow, and Blue Luminescence by Graphene Quantum Dots: Syntheses,  
30  
31 Mechanism, and Cellular Imaging. *ACS Appl. Mater. Interfaces* **2017**, *9*,  
32  
33 24846-24856.  
34  
35  
36  
37 (38) Bera, D.; Qian, L.; Tseng, T. K.; Holloway, P. H. Quantum Dots and Their  
38  
39 Multimodal Applications: A Review. *Materials* **2010**, *3*, 2260-2345.  
40  
41  
42  
43 (39) Leng, C.; Hung, H.-C.; Sun, S.; Wang, D.; Li, Y.; Jiang, S.; Chen, Z. Probing the  
44  
45 Surface Hydration of Nonfouling Zwitterionic and PEG Materials in Contact  
46  
47 with Proteins. *ACS Appl. Mater. Interfaces* **2015**, *7*, 16881-16888.  
48  
49  
50  
51 (40) Fu, Y. Y.; Guan, E. L.; Liang, J. G.; Ren, G. L.; Chen, L. Probing the Effect of  
52  
53 Ag<sub>2</sub>S Quantum Dots on Human Serum Albumin Using Spectral Techniques. *J.*  
54  
55  
56  
57  
58  
59  
60

1  
2  
3  
4  
5  
6  
7  
8  
9  
10  
11  
12  
13  
14  
15  
16  
17  
18  
19  
20  
21  
22  
23  
24  
25  
26  
27  
28  
29  
30  
31  
32  
33  
34  
35  
36  
37  
38  
39  
40  
41  
42  
43  
44  
45  
46  
47  
48  
49  
50  
51  
52  
53  
54  
55  
56  
57  
58  
59  
60

*Nanomater.* **2017**, *2017*, 1-7.

(41) Fan, R. J.; Sun, Q.; Zhang, L.; Zhang, Y.; Lu, A. H. Photoluminescent Carbon Dots Directly Derived from Polyethylene Glycol and their Application for Cellular Imaging. *Carbon* **2014**, *71*, 87-93

(42) Xiao, D.; Pan, R.; Li, S.; He, J.; Qi, M.; Kong, S.; Gu, Y.; Lin, R.; He, H. Porous Carbon Quantum Dots: One Step Green Synthesis Vial-Cysteine and Applications in Metal Ion Detection. *RSC Adv.* **2015**, *5*, 2039-2046.

(43) Bao, L.; Zhang, Z. L.; Tian, Z. Q.; Zhang, L.; Liu, C.; Lin, Y.; Qi, B.; Pang, D. W. Electrochemical Tuning of Luminescent Carbon Nanodots: from Preparation to Luminescence Mechanism. *Adv. Mater.* **2011**, *23*, 5801-5806.

(44) Fan, Z. J.; Kai, W.; Yan, J.; Wei, T.; Zhi, L. J.; Feng, J.; Ren, Y. M.; Song, L. P.; Wei, F. Facile Synthesis of Graphene Nanosheets via Fe Reduction of Exfoliated Graphite Oxide. *ACS Nano* **2011**, *5*, 191-198.

(45) Zhang, H. J.; Chen, Y. L.; Liang, M. J.; Xu, L. F.; Qi, S. D.; Chen, H. L.; Chen, X. G. Solid-Phase Synthesis of Highly Fluorescent Nitrogen-Doped Carbon Dots for Sensitive and Selective Probing Ferric Ions in Living Cells. *Anal. Chem.* **2014**, *86*, 9846-9852.

(46) Li, C. M.; Zheng, L. L.; Yang, X. X.; Wan, X. Y.; Wu, W. B.; Zhen, S. J.; Li, Y. F.; Luo, L. F.; Huang, C. Z. DNA-AuNP Networks on Cell Membranes as a Protective Barrier to Inhibit Viral Attachment, Entry and Budding. *Biomaterials*

1  
2  
3  
4  
5  
6  
7  
8  
9  
10  
11  
12  
13  
14  
15  
16  
17  
18  
19  
20  
21  
22  
23  
24  
25  
26  
27  
28  
29  
30  
31  
32  
33  
34  
35  
36  
37  
38  
39  
40  
41  
42  
43  
44  
45  
46  
47  
48  
49  
50  
51  
52  
53  
54  
55  
56  
57  
58  
59  
60

2016, 77, 216-226.

(47) Lin, N.; Hu, F.; Sun, Y.; Wu, C.; Xu, H.; Liu, X. Y. Construction of White-Light-Emitting Silk Protein Hybrid Films by Molecular Recognized Assembly among Hierarchical Structures. *Adv. Funct. Mater.* **2014**, *24*, 5284-5290.

(48) Chan, J. W.; Taylor, D. S.; Zwerdling, T.; Lane, S. M.; Ihara, K.; Huser, T. Micro-Raman Spectroscopy Detects Individual Neoplastic and Normal Hematopoietic Cells. *Biophys. J.* **2006**, *90*, 648-656.

(49) Stone, N.; Kendall, C.; Shepherd, N.; Crow, P.; Barr, H. Near-Infrared Raman Spectroscopy for the Classification of Epithelial Pre-Cancers and Cancers. *J. Raman Spectrosc.* **2002**, *33*, 564-573.

(50) Salman, A.; Shufan, E.; Zeiri, L.; Huleihel, M. Characterization and Detection of Vero Cells Infected with Herpes Simplex Virus Type 1 using Raman Spectroscopy and Advanced Statistical Methods. *Methods* **2014**, *68*, 364-370.

(51) Gonzalez-Navajas, J. M.; Lee, J.; David, M.; Raz, E. Immunomodulatory Functions of Type I Interferons. *Nat. Rev. Immunol.* **2012**, *12*, 125-135.

(52) Gomez, C. R.; Boehmer, E. D.; Kovacs, E. J. The Aging Innate Immune System. *Curr. Opin. Immunol.* **2005**, *17*, 457-462.

(53) Schoggins, J. W.; Rice, C. M. Interferon-Stimulated Genes and Their Antiviral Effector Functions. *Curr. Opin. Virol.* **2011**, *1*, 519-525.

- 1  
2  
3  
4 (54) Yu, Y.; Huang, X.; Liu, J.; Zhang, J.; Hu, Y.; Yang, Y.; Huang, Y.; Qin, Q. Fish  
5  
6 TRIM32 Functions as a Critical Antiviral Molecule against Iridovirus and  
7  
8 Nodavirus. *Fish Shellfish Immun.* **2017**, *60*, 33-43.  
9  
10  
11  
12  
13  
14  
15  
16  
17  
18  
19  
20  
21  
22  
23  
24  
25  
26  
27  
28  
29  
30  
31  
32  
33  
34  
35  
36  
37  
38  
39  
40  
41  
42  
43  
44  
45  
46  
47  
48  
49  
50  
51  
52  
53  
54  
55  
56  
57  
58  
59  
60

Abstract Graphic

